Automatic Detection and Segmentation of Large Lung Cancers from Chest CT Images

Jinghao Zhou[1], Sukmoon Chang[1,2], Qingshan Liu[1], Dimitris N. Metaxas[1], Binsheng Zhao[3], Michelle S. Ginsberg[3], and Lawrence H. Schwartz[3]

[1] CBIM, Rutgers, The State University of New Jersey, NJ, USA,
jhzhou@eden.rutgers.edu, {qsliu, dnm}@cs.rutgers.edu
[2] Computer Science, Capital College, Penn State University, Middletown, USA,
sukmoon@psu.edu
[3] Department of Radiology, Memorial Sloan-Kettering Cancer Center, NY, USA
{zhaob, schwartl, ginsberm}@mskcc.org

Abstract. Response assessment is critical for cancer patient management and new drug approval. Traditional methods to assess the response are based on measuring tumor size changes in one or two dimensions on computed tomography (CT) before and after therapy, and can be biased. In order to investigate if changes in tumor volume can better assess therapy response, there is an urgent need to develop accurate and reproducible computer-aided tools. Automatic detection and segmentation of lung cancers is a difficult task as lung cancers are often large in size, irregular in shape, and can grow against surrounding structures of similar density and intensity. In this paper, we propose a novel method for automatic segmentation of lung areas that can be distorted by large lung cancers using robust active shape models. We also propose a novel method for automatic detection and segmentation of large lung cancers using a supervised learning framework followed by the analysis of 3D texture likelihood maps. Finally, we present promising results of our methods applied to different clinical applications. The proposed computer-aided methods may provide a new powerful tool for accurate and reproducible quantification of tumor volumes in lung cancer clinical trials.

1 Introduction

The evaluation of therapy response is critical for determining whether a particular treatment is effective on a specific cancer type in a patient. Traditionally, the ways to assess the response are based on measuring size changes of cancer in a transverse image using computed tomography (CT) before and after a treatment [1, 2]. However, the traditional uni-dimensional (maximal diameter of tumor) and bi-dimensional (product of maximal diameter and its perpendicular maximal diameter) measurements can be biased especially when a tumor is not spherical in shape and does not change its shape in a spherical fashion. The preliminary result in a lung cancer study [3] showed that the changes in

tumor volume could be determined as early as 3 weeks after a novel chemotherapy, whereas the changes of tumor volume measured in the traditional methods were significantly less sensitive in the same time period. In addition, manual delineation of tumor contours is time-consuming and lacks the reproducibility. Therefore, there is an urgent need for automatic detection and accurate segmentation methods for the volumetric assessment of therapy response.

Unlike small lung nodules, lung cancers to be treated are often large in size, present spiculate edges, and grow against surrounding structures such as the chest wall, the mediastinum, and blood vessels, which make automatic detection and segmentation difficult [3]. Thus, the algorithms developed for automatic detection and segmentation of small solid lung nodules are most likely to fail when applied to large lung cancers [4–13]. In those studies, larger lung lesions that were attached to the chest wall and mediastinum could be easily and mistakenly excluded from the segmented lungs in which the subsequent lesion detection would be performed [4–7]. Also, the existing segmentation algorithms often assumed that small lung nodules would possess spherical shape, which is not adequate for describing large lung cancers. Furthermore, inability to separate a larger lesion from its surrounding structures of similar intensities was another shortcoming of the existing segmentation algorithms.

In this paper, we propose novel methods for automatic segmentation of lung areas as well as automatic detection and segmentation of large lung cancers from CT images for the purpose of therapy response assessment. We first propose a robust active shape model for the accurate segmentation of lung areas that are distorted and occluded by large lung cancers. Next, we develop a classifier for the detection of cancers in the segmented lung areas by boosting a k-Nearest Neighbor (k-NN) classifier, whose distance measure is the Euclidean distance between the nonparametric density estimates of two regions. The statistical validation of the proposed classifier is also provided. Finally, the classified cancers are automatically segmented by analyzing 3D texture likelihood maps of the surrounding areas. We present the promising experimental results of our method applied to various clinical data. The proposed methods would provide a new powerful tool for automatic detection as well as accurate and reproducible segmentation of lung cancers for therapy response assessment in lung cancers.

2 Method

2.1 Robust active shape models (RASM) for lung area segmentation

Large lung cancers often grow against surrounding structures, such as the chest wall and mediastinum. Lung areas that are distorted and occluded by such lesions are hard to segment due to the similarity of the intensities between the cancers and the surrounding structures in CT images. In this section, we develop a robust method to accurately segment lung areas occluded by large cancers by improving the active shape model framework.

An active shape model (ASM) represents the shapes of interest as a Point Distribution Model (PDM) [14]. Then, it constructs a shape space as a set of

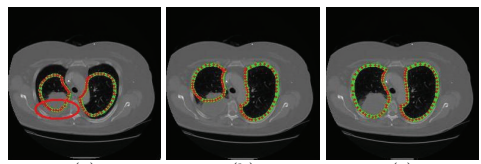

(a) (b) (c)

Fig. 1. The segmented lung area using RASM. Red points are active shape model and green lines are the connected contour. (a) Large cancers attached to the chest wall and mediastinum (large red circle) and the initialization of the ASM, (b) ASM finding the false boundary of lung, and (c) RASM finding the correct boundary of lung and the large white area in the left lung is a large lung cancer.

orthogonal basis $\boldsymbol{P}$ by applying the Principal Component Analysis (PCA) and finds an optimal shape for a new example of the shapes with PCA reconstruction. Given the shape space $\boldsymbol{P}$, the projection $\boldsymbol{C}$ of a new example shape $\boldsymbol{X}$ is given as $\boldsymbol{C} = \boldsymbol{P}^T d\boldsymbol{X}$, where $d\boldsymbol{X} = \boldsymbol{X} - \bar{\boldsymbol{S}}$ and $\bar{\boldsymbol{S}}$ is the mean shape from the aligned shapes of the training set. Based on the projection $\boldsymbol{C}$, we can easily find a corresponding shape in the shape space as $\tilde{\boldsymbol{X}} = \boldsymbol{PC} + \bar{\boldsymbol{S}}$. For simplicity, we denoted $d\tilde{\boldsymbol{X}} = \boldsymbol{PC}$. Since $\bar{\boldsymbol{S}}$ is constant, the accuracy of $\tilde{\boldsymbol{X}}$ depends on $\boldsymbol{C}$ which is related to $d\boldsymbol{X}$. In many applications, $d\boldsymbol{X}$ is often optimized with some low-level image features such as the gradient along normal directions to the boundary of an initial shape toward the strongest edge in the image [14].

The ASM method as described above, however, is not suitable for the accurate segmentation of lung areas with large cancers attached on their walls, since the cancers occlude the real boundary of the lung and appear as the strongest edge, as illustrated in Fig. 1(a) and (b). To overcome this difficulty, we develop a robust ASM (RASM) based on the robust M-estimator [15]. The goal is to recover the projection $\boldsymbol{C}$ with the majority of the correct $d\boldsymbol{X}$ and to restrain the outlier points of $d\boldsymbol{X}$. Mathematically, it computes $\boldsymbol{C}$ by minimizing the following robust energy function:

$$\boldsymbol{E}_{rpca}(\boldsymbol{C}) = \min_{\boldsymbol{C}} G\left(\|d\boldsymbol{X} - \boldsymbol{PC}\|, \sigma\right) \tag{1}$$

where, $G(x, \sigma) = x^2/(x^2 + \sigma^2)$ is the Geman-McClure error function and σ is a scale parameter that controls the convexity of the robust function. The solution for $\boldsymbol{C}$ can be obtained by an iterative gradient descent search on $\boldsymbol{E}_{rpca}$:

$$\boldsymbol{C}^{(n+1)} = \boldsymbol{C}^{(n)} + \lambda \Delta \boldsymbol{C} \tag{2}$$

where, λ is a small constant that determines the step size and

$$\Delta \boldsymbol{C} = \frac{\partial \boldsymbol{E}_{rpca}}{\partial \boldsymbol{C}} = -2\boldsymbol{P}(d\boldsymbol{X} - \boldsymbol{PC}) \frac{\sigma^2}{(\|d\boldsymbol{X} - \boldsymbol{PC}\|^2 + \sigma^2)^2}$$

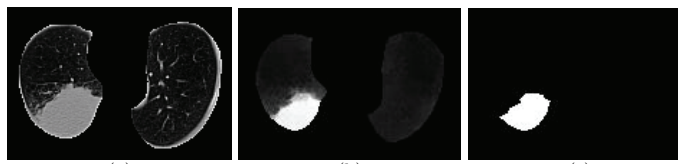

(a) (b) (c)

Fig. 2. Effects of F_{cyl} (only one slice from the whole volume is shown). (a) Original volume, (b) Volume filtered with F_{cyl}, and (c) Volume after thresholding.

The iterative process is performed until $\|\boldsymbol{E}_{rpca}^{(t+1)} - \boldsymbol{E}_{rpca}^{(t)}\| < \epsilon$, where ϵ is a pre-selected tolerance. Using the robust projection $\boldsymbol{C}^*$, we obtain a robust shape in the shape space as:

$$\tilde{\boldsymbol{X}} = \boldsymbol{P}\boldsymbol{C}^* + \bar{\boldsymbol{S}}$$

The result of this process is illustrated in Fig. 1(c), where the lung area occluded by a large lesion is accurately segmented.

2.2 Detection of large lung cancers

In this section, we present a novel method for automatic detection of large lung cancers from the segmented lung areas. The method is based on 3D texture analysis using a machine learning framework, i.e., boosting the k-NN classifier. However, the accuracy of the detection may be hindered by various structures within a lung. Thus, we first apply a 3D cylinder filter to suppress the intensity values of vessels and other elongated structures as well as noise inside a lung, while maintaining the intensity values of large lung cancers intact [16, 17]. The cylinder filter F_{cyl} is defined as:

$$F_{\text{cyl}}(x) = \min_{\theta} \left(\min_{y \in \Omega_{\theta}^{x}} I(y) \right)$$

where, Ω_{θ}^{x} is the domain of the cylinder filter centered at x with orientation θ. F_{cyl} is a hybrid minimum neighborhood filter that produces strong responses to large blob-like objects (e.g., large cancers). In this paper, we have selected the parameters of F_{cyl} empirically and used a cylinder with radii of 1, 2 and 3 voxels and length of 7 voxels at 7 different orientations. In Fig. 2(a) and (b), we can see that vessels and noise are effectively suppressed while the large lung cancers remains intact. After the filtering, we isolate the candidate regions for large lung lesions by simple thresholding (Fig. 2(c)). The threshold value is automatically determined by analyzing the histogram of the filter response image [16]. Each candidate region is then classified with a learning framework described below.

To apply a supervised learning framework, we collected volumetric samples for positive (lesion) and negative (non-lesion) examples manually. Let Ψ_M be the

region of a volumetric sample bounded by a sphere. We estimate the probability density function (pdf) of the intensity values of the interior of Ψ_M. We use a nonparametric kernel based method to approximate the pdf. Let $i \in [0, 255]$ denote the random variable for intensity values. The intensity pdf of Ψ_M is defined as:

$$P(i|\Psi_M) = \frac{1}{V(\Psi_M)} \iiint_{\Psi_M} \frac{1}{\sqrt{2\pi\sigma^2}} \exp\left(-\frac{(i - I(y))^2}{2\sigma^2}\right) dy \tag{3}$$

where, $V(\Psi_M)$ denotes the volume of Ψ_M, y are the voxels in the domain Ψ_M, and σ is the standard deviation of a Gaussian kernel.

For the candidate areas of large cancers isolated above, the learning for their classification has a discrete target function $f : \mathcal{R}^n \mapsto \{\oplus, \ominus\}$, with the label $\oplus$ for lesions and $\ominus$ for non-lesions. For k-NN, an instance $\boldsymbol{x}$ is represented as a point in $\mathcal{R}^n$ by a feature vector $\langle a_1(\boldsymbol{x}), \cdots, a_n(\boldsymbol{x})\rangle$, where $a_i(\boldsymbol{x}) = P(i|\Psi_M)$. The Euclidean distance is used as the distance measure between two instance vectors. Given a query instance $\boldsymbol{x}_q$ to be classified, k-NN returns $\hat{f}(\boldsymbol{x}_q)$, as its estimate of $f(\boldsymbol{x}_q)$, which is the most common value of f among the k training instances nearest to $\boldsymbol{x}_q$, that is, $\hat{f}(\boldsymbol{x}_q) = \arg\max_{v \in \{\oplus,\ominus\}} \sum_{i=1}^{k} \delta(v, f(\boldsymbol{x}_i))$, where $x_1, \cdots, x_k$ denote the k instances from training samples that are nearest to $\boldsymbol{x}_q$, and $\delta(a, b) = 1$ if $a = b$ and 0 otherwise. To obtain an accurate classification, k-NN requires a large training set, which results in slow classification due to the large number of distance calculations. We overcome this difficulty by boosting k-NN [18]. As in [18], our purpose for boosting k-NN is to improve the speed of k-NN by reducing the number of prototype instances and thus reducing the required number of distance calculation without affecting the error rate.

2.3 Segmentation of large lung cancers

We now segment the classified large lung cancers. Because of the hazy appearance and irregular shape of large lung cancers and the large overlap of intensity values between large lung cancers and surrounding vessels, simple thresholding and contour based segmentation method do not provide accurate segmentation. The proposed method involves the analysis of a 3D texture likelihood map using a nonparametric density estimation [19], followed by eigenanalysis of the Hessian matrix to accurately remove vessels overlapped with large lung lesions.

We extract the region of interest (ROI) surrounding a classified large lung cancer based on the detection of the large lung cancers. For each voxel in the ROI, we evaluate the likelihood of the voxel belonging to a large lung cancer by measuring the 3D texture consistency between the large lung cancer and a small spherical region (i.e., 3D texon) centered at the voxel.

Let Φ_M be the region of a volumetric sample of a classified large lung cancer bounded by a sphere. Using (3), we estimate the pdf of the intensity values of the interior of Φ_M, i.e., $p_M = P(i|\Phi_M)$. Similarly, let Φ_T be the region of the 3D texon centered at the given voxel in the ROI. Again using (3), we also estimate

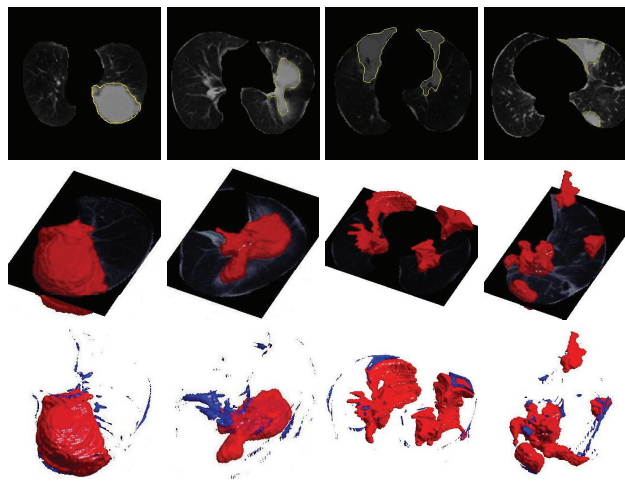

Fig. 3. Results. Segmented large lung cancers projected onto a slice (top), 3D reconstruction of large lung cancers (middle and bottom).

the pdf of the interior of Φ_T, i.e., $p_T = P(i|\Phi_T)$. To measure the similarity between the two pdfs, we use an information theoretic distance measure called Kullback-Leibler Divergence (KLD) [20]. The Bhattacharya distance, which is a symmetrized variation of KLD, between Φ_M and Φ_T is:

$$B(p_M \| p_T) = -\log \rho(p_M \| p_T) = -\log \int [p_M(i)]^{\frac{1}{2}} [p_T(i)]^{\frac{1}{2}} \, di$$

We evaluate the 3D texture likelihood of the 3D texon at every voxel in ROI. We define this likelihood using ρ, since it increases as the Bhattacharya distance between two distributions decreases. The radius of a 3D neighborhood sphere used in our paper is less than 3 voxels and the model interior texture is mostly homogeneous with some level of noise. Thus, it is not necessary to consider the spatial correlation between voxels. Finally, we remove the remaining vessels around large lung cancers in the 3D likelihood map by using the eigenanalysis of the Hessian matrix [21–23]

3 Results

We have 10 chest CT images containing 16 large lung cancers. To test the proposed method, we collected 500 volumetric samples, containing 300 training samples and 200 testing samples, from 4 training clinical chest CT images. The

samples were of size $15 \times 15 \times 3$ voxels from the CT volumes. Each sample was converted to an instance vector in $\mathcal{R}^{256}$, representing its nonparametric density estimate. For the boosted k-NN, we used the standard Euclidean distance as the distance measure between two instances as described in Section 2.2. We performed bootstrapping to estimate the generalization error of our large lesion detection method [24]. We trained and tested the proposed method on bootstrap samples. After 20 steps of boosting, the mean error rate converged to 3.50%.

We applied the trained classifier to all 10 CT volumes containing 16 large lung cancers. The CT volumes were acquired by multi-slice HRCT scanners with 5mm slice collimation. The number of slices in each CT scan ranged from 44 to 69 (and digitally resliced to obtain cubic voxels, resulting in 130 to 205 slices), each of which are of size 512×512 pixels, with in-plane resolution of 0.82mm. The classifier detected all 16 lesions successfully with no false negatives (Fig. 3). However, it also detected 2 false positive lesions, which the trained radiologists classified as atelectases.

The detected large lung cancers were then segmented using the method described in Section 2.3. Fig. 3 illustrates four representative cases of the segmented large lung cancers. In the figure, the 3D reconstruction of the segmented 3D large lung cancers (middle and bottom row) as well as their 2D projections on one of the slices (top row) are shown. From the figure, we can also see that the surrounding vessels are accurately removed from the large lung lesions segmented. Table 1 compares the greatest diameters, their greatest perpendicular diameters and tumor volumes of the 16 lung cancers from the results of the manual segmentation by experts and the automatic segmentation by the proposed method. The table shows that the mean relative error of the greatest diameter and its greatest perpendicular diameter are 2.8% and 2.2% and shows that the mean relative error of the tumor volume is 8.4%. We also compared the overlapping ratios of the tumor regions segmented manually and automatically, which ranged from 80.9% to 97.3%. The low overlapping ratios were resulted from the cases in which the cancers were heavily occluded by blood vessels, where the expert radiologists also found difficulty. The mean overlapping ratio was 90.9%. These results demonstrate the potential of our method to correctly segment occluded lung areas as well as the accuracy of the classification and segmentation of the large lung cancers. These results demonstrate the potential of our method to correctly segment occluded lung areas as well as the accuracy of the classification and segmentation of the large lung cancers.

4 Discussion

Lung cancers to be treated are often large in size and grow against surrounding structures such as chest wall, mediastinum, and blood vessels. Large lung cancers attached to such structures make it difficult to accurately segment lung areas from chest CT images, since they occlude the real boundary of the lungs and have similar intensity values to the surrounding structures. In this paper, we proposed a novel method for automatic and accurate segmentation of lung areas

Table 1. Comparisons. $d1$ and $d2$ are the greatest diameter and its greatest perpendicular distance of each tumor. Vol is the volume of each tumor. Overlap ratio is the volume overlap ratio of the manual segmentation results and automatic segmentation results. Manual and Auto are the measurements on the manual segmentation results and the automatic segmentation results, respectively.

Dataset	**d1** (mm)		**d2** (mm)		**Vol** (mm^3)		**Overlap Ratio** (%)
	Manual	Auto	Manual	Auto	Manual	Auto	
1	95	94	37	36	9676	9043	92.5
2	74	73	35	33	13357	12237	90.2
3	84	83	25	24	12704	11753	91.2
4	34	35	32	33	1643	1819	93.6
5	21	20	16	16	278	254	92.1
6	13	13	11	11	305	291	92.5
7	15	16	13	13	462	503	90.0
8	51	52	18	18	2152	2228	91.6
9	21	20	12	12	258	235	82.2
10	21	20	19	18	1402	1226	97.3
11	7	7	7	6	61	57	80.9
12	68	67	59	58	5988	5583	94.3
13	36	37	27	28	6268	6783	91.4
14	22	23	13	13	291	320	88.3
15	27	26	17	16	657	591	95.6
16	39	38	33	32	4583	4212	91.6
mean error (%)	2.8		2.2		8.4		90.9

that were distorted and occluded by large lung cancers using robust active shape models.

We also proposed a novel method for the automatic detection and segmentation of large lung cancers from chest CT images. The proposed method first extracted candidate lung cancer areas by applying the 3D cylinder filter. Then, each candidate region was classified by boosting the k-NN, whose distance measure was the Euclidean distance between the two intensity pdfs. We performed bootstrapping to estimate the generalization error of the method and showed the mean error rate of the method converged to 3.50%. Each cancer detected was automatically segmented by analyzing the texture likelihood map of the region.

The very promising results of our methods applied to various clinical chest CT images were also presented. Although the evaluation of therapy response is critical for determining whether a particular treatment is effective on a specific cancer type in a patient, the traditional methods such as uni-dimensional and bi-dimensional measurements of tumor size are not sensitive enough to accurately evaluate the changes in tumor volumes. In addition, the manual delineation of cancer contours is time-consuming and lacks the reproducibility. The proposed methods provides a new powerful tool for automatic detection as well as accu-

rate and reproducible segmentation of large lung cancers for therapy response assessment in lung cancers.

References

1. Miller, A., Hogestraeten, B., Staquet, M., et al.: Reporting results of cancer treatment. Cancer **47** (1981) 207–214
2. Therasse, P., Arbuck, S., Eisenhauer, E., et al.: New guidelines to evaluate response to treatment in solid tumors. J. Natl. Cancer Inst. **92** (2000) 205–216
3. Zhao, B., et al.: Lung Cancer: Computerized Quantification of Tumor Response—Initial Results. Radiology **241** (2006) 892–898
4. Armato III, S., Giger, M., MacMahon, H.: Automated detection of lung nodules in CT scans: Preliminary results. Medical Physics **28**(8) (2001) 1552–1561
5. Brown, M., et al.: Patient-specific models for lung nodule detection and surveillance in CT images. IEEE Trans. Med. Imag. **20**(12) (2001) 1242–1250
6. Lee, Y., et al.: Automated detection of pulmonary nodules in helical CT images based on an improved template-matching technique. IEEE Trans. Med. Imag. **20**(7) (2001) 595–604
7. Takizawa, H., et al.: Recognition of lung nodules from X-ray CT images using 3D Markov Random Field models. In: Int. Conf. Pattern Recog. Volume 1. (2002) 10099
8. Zhao, B., et al.: Automatic detection of small lung nodules on ct utilizing a local density maximum algorithm. J. Appl. Clin. Med. Phys. **4**(3) (2003) 248–260
9. Zhao, B., et al.: Two-dimensional multi-criterion segmentation of pulmonary nodules on helical ct images. IEEE Trans. Med. Imag. **22**(10) (2003) 1259–1274
10. Boscolo, R., Brown, M., McNitt-Gray, M.: Medical image segmentation with knowledge-guided robust active contours. RadioGraphics **33** (2002) 437–448
11. Ko, J.P., et al.: Small pulmonary nodules: volume measurement at chest ct—phantom study. Radiology **228** (2003) 864–870
12. Kostis, W., et al.: Three-dimensional segmentation and growth rate estimation of small pulmonary nodules in helical ct images. IEEE Trans. Med. Imag. **22**(10) (2003) 1259–1274
13. Chang, S., Zhou, J., Dimitris Metaxas, L.A.: False-positive elimination for computer-aided detection of pulmonary micronodules. In: SPIE Internation Symposium on Medical Imaging. (2006) 1751–1758
14. Cootes, T., Taylor, C., Cooper, D., Graham, J.: Active shape models—their training and application. Comp. Vis. Imag. Under. **61**(1) (1995) 38–59
15. De La Torre, F., Black, M.: A framework for robust subspace learning. Int. J. Comput. Vis. **54**(1-3) (2003) 117–142
16. Chang, S., Emoto, H., Metaxas, D., Axel, L.: Pulmonary micronodule detection from 3d chest ct. In: MICCAI. (2004) 821–828
17. Zhou, J., Chang, S., Metaxas, D., Zhao, B., Schwartz, L.H., Ginsberg, M.S.: Automatic detection and segmentation of ground glass opacity nodules. International conference on Medical Image Computing and Computer Assisted Intervention (MICCAI) (2006) 784–791
18. Freund, Y., Schapire, R.: Experiments with a new boosting algorithm. In: ICML. (1996) 145–156
19. Huang, X., Qian, Z., Huang, R., Metaxas, D.: Deformable-model based textured object segmentation. In: EMMCVPR. (2005) 119–135

20. Ali, A., Silvey, S.: A general class of coefficients of divergence of one distribution from another. J. Roy. Stat. Soc., **28** (1966) 131–142
21. Lorenz, C., et al.: Multi-scale line segmentation with automatic estimation of width, contrast and tangential direction in 2d and 3d medical images. In: CVRMed-MRCAS. (1997) 233–242
22. Zhou, J., Chang, S., Metaxas, D., Axel, L.: Vessel boundary extraction using ridge scan-conversion and the deformable model. In: ISBI. (2006) 189–192
23. Zhou, J., Chang, S., Metaxas, D., Axel, L.: Vascular structure segmentation and bifurcation detection. IEEE International Symposium on Biomedical Imaging (2007) 872–875
24. Efron, B.: Estimating the error rate of a prediction rule: Improvement on cross-validation. J. Amer. Stat. Assoc. **78** (1983) 316–331